ISSN: 2476- 2334

Research Article

International Journal of Nanotechnology & Nanomedicine

Room Temperature Synthesis of Monodisperse ZnO Nanoparticles Using Ultrasonically Atomized Precursor Mist in Simple Chemical Route

DG Patil, SD Bagul, PS Sonawane, LA Patil and MS Wagh*

Nanomaterials Research Lab, P. G. Department of Physics, Pratap College Amalner 42540, India

***Corresponding author**
MS Wagh, Associate Professor, Nanomaterials Research Lab, P. G. Department of Physics, Pratap College Amalner 42540, India. E-mail: wmadhav19@yahoo.co.in

Submitted: 03 Aug 2019; **Accepted**: 07 Aug 2019; **Published**: 12 Aug 2019

Abstract

Monodisperse zinc oxide (ZnO) nanoparticles were synthesized using ultrasonically atomized precursor mist in simple chemical route at low temperature. Analytical grade sodium hydroxide and zinc chloride were dissolved in 100 ml methanol. Zinc chloride precursor solution was converted into very fine mist (atomized) using a nozzle (Sono-Tek Corporation, U.S.A.) operated at ultrasonic frequency of 120 KHz. Fine mist droplets were added slowly (50ml/hour) into sodium hydroxide solution in 2 hours. The NaOH solution in beaker turned slowly into white product due to addition of zinc chloride. The white product was kept in constant temperature bath at 90°C for 3 hours. The white product was washed five times using double distill water and dried in oven for 2 hours. Different powder samples were synthesized using same procedure by changing the molarity of sodium hydroxide keeping the molarity of zinc chloride and other preparative conditions same. The structural, microstructural, thermal and optical properties of fine powders were analyzed using X Ray Diffractometer, Scanning Electron Microscopy, Simultaneous Thermal Analyzer, UV-Vis Spectroscopy and Photoluminescence Spectroscopy. Fine ZnO nanorods, elongated and spherical nanoparticles were observed due to change in molarity of NaOH. The results are discussed and interpreted.

Keywords: ZnO Nanoparticles, Fine Mist, Zn^{+}/OH^{-} Ratio, Methanol, Room Temperature Synthesis, Simple Chemical Route

Introduction

Due to its direct, wide band gap of 3.37 eV, ZnO has a wide range of applications in optoelectronic devices, such as, light-emitting diodes, photodetectors, and p-n homojunctions. The large Exciton binding energy of 60 meV, compared to that of GaN (approximately 25 meV), enhances the luminescence efficiency of the emitted light even at room temperature and higher [1, 2]. The visible photoluminescence (PL) at approximately 2.5 eV (approximately 495 nm) originated from intrinsic defects, makes ZnO suitable for applications in field emission and vacuum fluorescent displays [3]. Many techniques including hydrothermal synthesis, pulsed laser deposition, sputtering, molecular beam epitaxy, chemical vapor deposition and oxidation of metallic zinc powder have been used to prepare ZnO in different forms and structures for various applications [4-10]. Nanoparticulate form enhances the catalytic activity due to its large surface area, presence of vacancies and uncoordinated atoms at corners and edges. The photocatalytic activity is also improved by band gap engineering, as a result of the quantum confinement effect [11-13]. There are number of research articles published on applications of nanomaterials in renewable energy and in enhancing the performance of the direct absorption solar collectors [14-22]. A well-controlled synthesis process at room temperature is needed for the economical use of ZnO in applications such as water treatment and other environmental applications. Present article reports a direct, simple, room-temperature synthesis method for ZnO nanoparticles using sodium hydroxide (NaOH) as a precipitating agent, zinc chloride as a zinc precursor, and methanol as a solvent.

Materials and Methods

Analytical grade (Merck) zinc chloride (ZnCl2) and sodium hydroxide (NaOH) were used to synthesize zinc oxide nanoparticles. Zinc chloride (0.25M) and sodium hydroxide (2.5M) solutions (100ml each) were prepared in methanol.

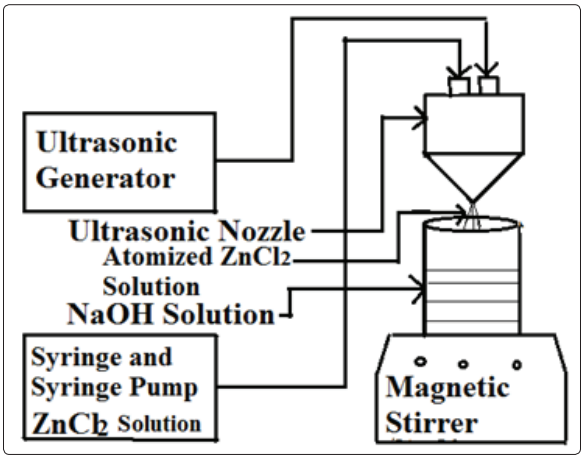

Figure 1: Ultrasonically atomized precursor assisted simple chemical route

Sodium hydroxide was taken in 250ml beaker. Zinc chloride was atomized using ultrasonic nozzle (Sono-Tek Corporation, U.S.) operated at ultrasonic frequency of 120KHz before adding to sodium hydroxide solution. 50 ml zinc chloride was taken in syringe. The syringe was placed in syringe pump (Figure 1). The syringe pump was used to push the piston of syringe slowly so that the zinc chloride solution was delivered to nozzle with constant speed of 50ml/hour. The nozzle converted the solution into fine spray of droplets. The atomized zinc chloride was allowed to pass slowly into sodium hydroxide (NaOH) solution in beaker. The beaker solution was continuously stirred without heating while adding the zinc chloride droplets. The mixture solution in beaker was observed to be turning slowly into white product. Slow addition of zinc chloride in the form of fine droplets was to avoid fast precipitation, to keep the speed of chemical reaction slow, to keep control on ZnO nucleation and to keep growth rate of nuclei low to form ZnO nanocrystalline particles. The beaker with white product was placed in constant temperature bath at temperature of 90°C for 3 hours. The product was then washed five times using double distill water and dried at 100oC in oven. The sample so obtained was termed as SDB5. Different ZnO powders were synthesized using the same procedure above, keeping molarity of zinc chloride same (0.25M) and changing molarity of sodium hydroxide as: 2.0.M, 1.25M, 1.0M, 0.5M, 0.25M and 0.1M. The powder samples so prepared were termed respectively as: SDB6, SDB7, SDB9, SDB8, SDB10 and SDB11.

Results

Structural analysis of ZnO Nanoparticles

The structural analysis of ZnO powders was carried out using Rigaku's MiniFlex 600 Bench top XRD Diffractometer (XRD) with CuKα radiation of wavelength of 1.5418 Å. Figure 2 shows XRD patterns of as prepared samples. Observed XRD patterns of SDB5, SDB6, SDB7, SDB9 and SDB8 samples match exactly with peaks reported in standard JCPDS data (JCPDS 36-1451). The XRD patterns confirmed the powders to be the Wurtzite hexagonal phase of ZnO. AS prepared SDB10 (0.1M $ZnCl_2$ and SDB11 (0.25 M ZnCl2) samples (See XRD pattern of SDB10 in Fig 2) do not match with peaks of XRD pattern reported in standard JCPDS data (JCPDS 36-1451).

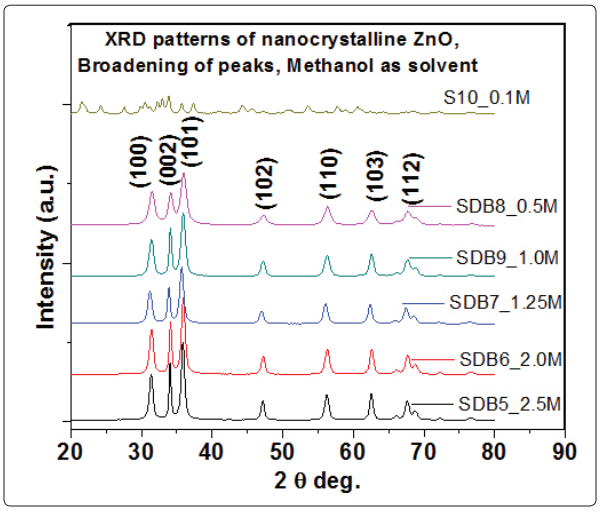

Figure 2(a): XRD patterns of nanostructuredZnO samples

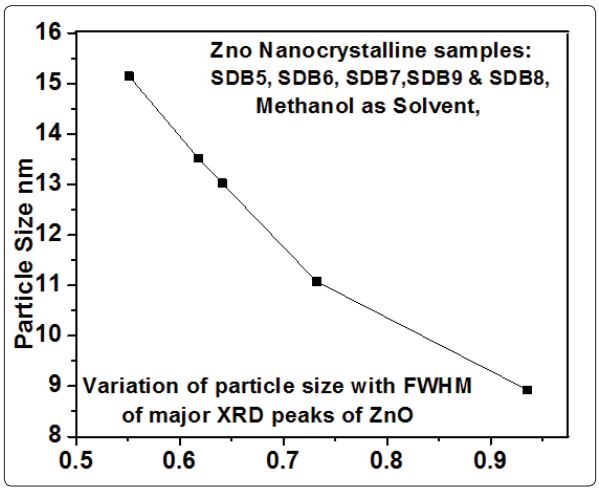

Figure 2(b): Variation of particle size with FWHM

Table 1: Broadening of peaks in ZnO XRD patterns and lattice constants

Sample name	2-theta (deg.)	d (ang.)	FWHM (deg.)	Nanoparticle Size (nm)	Lattice Parameters of ZnO unit cells			
					a Å	c Å	c/a	Volume VÅ^3
SDB5_2.5M	35.840	2.5035	0.551	15.15	3.293	5.264	1.5985	85.6
SDB6_2.0M	35.898	2.4995	0.618	13.52	3.285	5.255	1.5997	85.07
SDB7_1.25M	35.663	2.5155	0.641	13.023	3.31	5.290	1.5983	86.9
SDB9_1.0M	35.880	2.5008	0.732	11.08	3.287	5.258	1.5996	85.22
SDB8_0.5M	35.959	2.4955	0.936	8.923	3.2810	5.253	1.61	84.8
Average					3.2912	5.264	1.6012	85.52

It is clear from XRD patterns in figure 2(a) and the graph in figure 2(b) that the peak broadening (FWHM) increases with decrease in size of nanoparticles. Stable homogeneous wurtzite phase of ZnO was obtained upto NaOH molarity of 0.5 ($ZnCl_2$ 0.25M). When NaOH molarity was smaller than 0.5, different intermediate phases along with ZnO were resulted as shown in XRD pattern of SDB10 (Figure 2(a)). Molarity of NaOH in case of SDB10 was 0.1M. Structure related parameters of ZnO nanostructures are determined from XRD data and presented in (Table 1). Reported ZnO wurtzite structure has hexagonal unit cell with two lattice constants 'a' and 'c' in the ratio of c/a =1.633. Lattice constants ('a' and 'c') determined by experimental measurements and theoretical calculation for wurtzite ZnO are in good agreement with each other. Lattice constant 'a' range from 3.281 Å to 3.31 Å, lattice constant 'c' range from 5.253 Å to 5.290 Å and 'c/a' was in the range from 1.5983 to 1.61. The average ratio 'c/a' was observed to be 1.6012 which is approximately matching with ideal reported ratio (1.633). This indicates the formation of ideal wurtzite structure in experimentally prepared nanocrystalline powders.

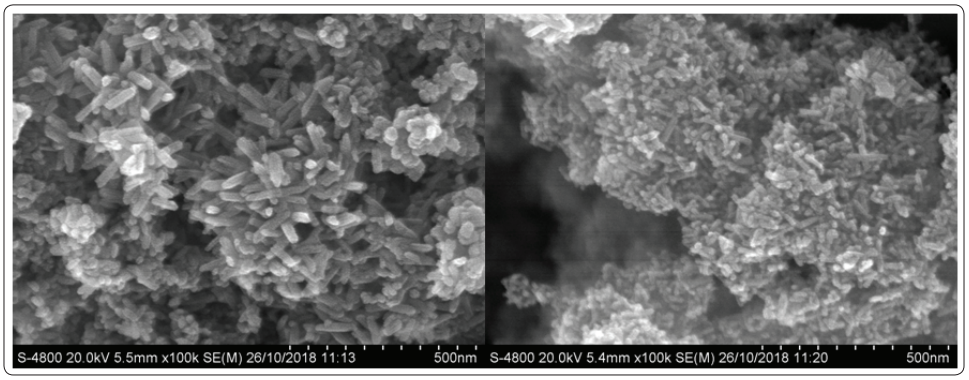

Figure 3(a): SEM image of SDB5_2.5M **Figure 3(b):** SEM image of SDB7_1.25M

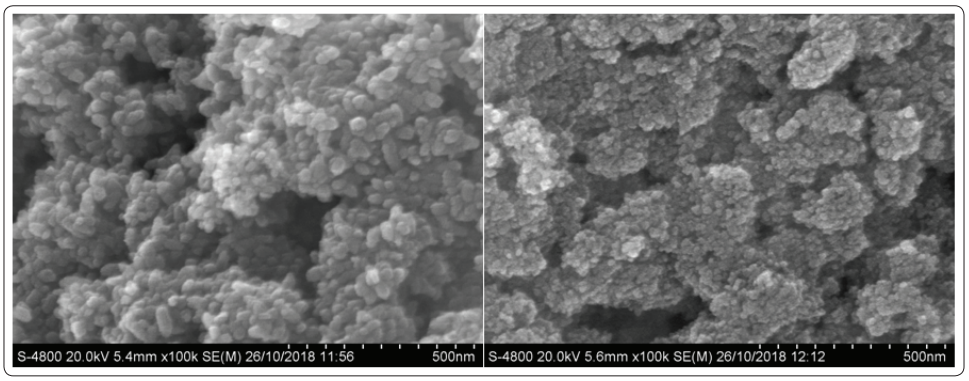

Figure 3(c): SEM image of SDB9_1.0M **Figure 3(d):** SEM image of SDB8_0.5M1.25M

Figures 3(a), (b), (c) and (d) represent SEM images respectively for NaOH molarities of: 2.5M, 1.25M, 1.0M and 0.5M. Figures 3(a) and (b) show ZnO nanorods, Figure 3(c) shows elongated nanoparticles, and Figure 3(d) shows spherical nanoparticles. The change in morphology and size of ZnO nanocrystallites may be due to change in molarity of NaOH. When molarity of NaOH changes, there is the change in relative concentrations of free Zn^{2+}, OH^-, Na^+ ions and the solution pH (Table 2). The change in solution pH would influence on formation of ZnO nucleation centres, $Zn(OH)_2$ colloids and growth units $(Zn(OH)_4^{2-}$ in solution.

Table 2: Morphology and size of ZnO nanostructures with change in molarity of NaOH

Sample Name	NaOH	pH of solution	EDAX at. %		Morphology	Average Dimensions of nanostructures		
			Zn	O		Length (L) nm	Diameter/ Width (D) nm	Aspect Ratio (A)
SDB5	2.5M	10.8	80.96	19.04	Nanorods	79	26	3.76
SDB7	1.25M	9.9	31.01	68.99	Nanorods	74.	16	4.63
SDB9	1.0M	9.5	31.13	68.87	Elongated nanoparticles	28	22	1.68
SDB8	0.5M	9.3	33.0	67.0	Spherical nanoparticles	Average Diameter= 13nm		

ZnO nanoparticles of spherical morphology with diameter ranging from 7 to 19 nm (average size of = 13nm) were observed (Figure 3(d)) when molarity of NaOH was 0.5M, the solution pH was 9.3 and methanol was used as solvent. These were the optimum conditions favorable for obtaining ZnO nanoparticles. Moreover, this process is well repeatable and easily controllable.

The average length and diameter of the nanorods in SDB5 sample are larger than the average length and diameter of nanorods in SDB7 sample. The aspect ratio of SDB7 sample is larger than an aspect ratio of SDB5 sample. The tendency to grow along c axis of ZnO rods is common but the lengths and diameters of SDB5, SDB7 and SDB9 samples are decreasing. It may be due to gradual decrease of growth units $Zn(OH)_4^{2-}$ in solutions respectively from SDB5, SDB7 and SDB9 samples.

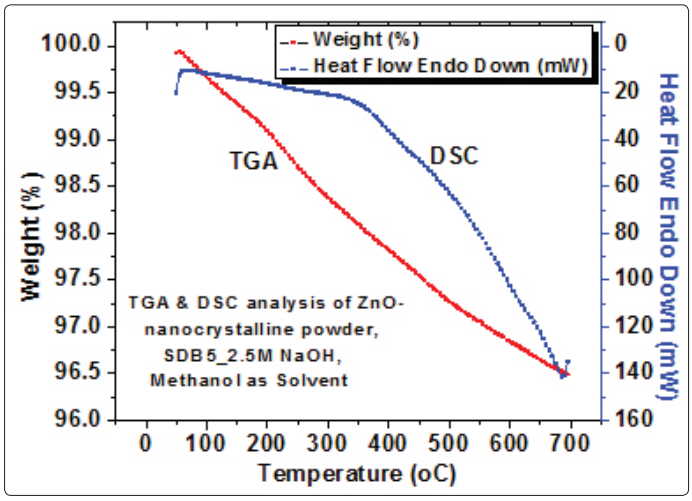

Figure 4(a): TGA & DSC curves of SDB5

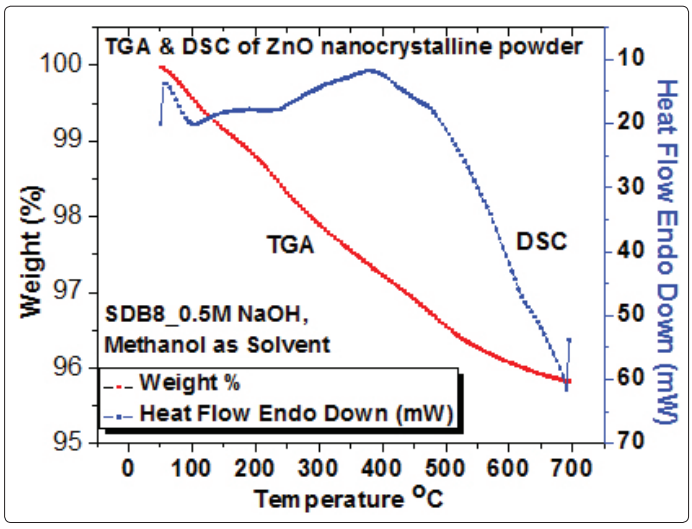

Figure 4(b): TGA & DSC curves of SDB8

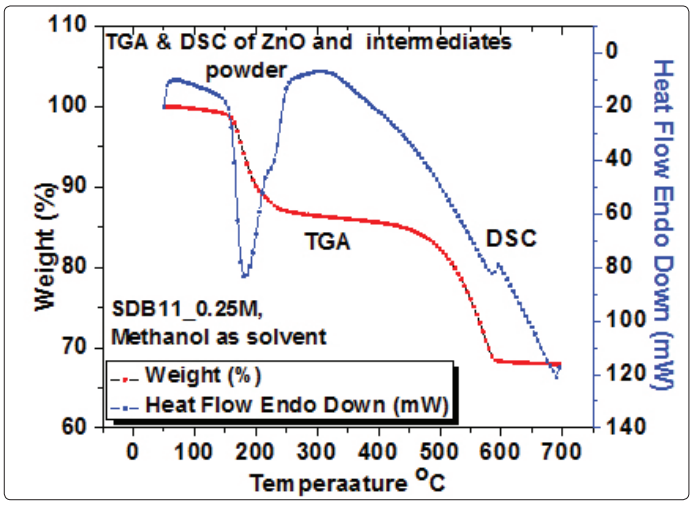

Figure 4(c): TGA & DSC curves of SDB11

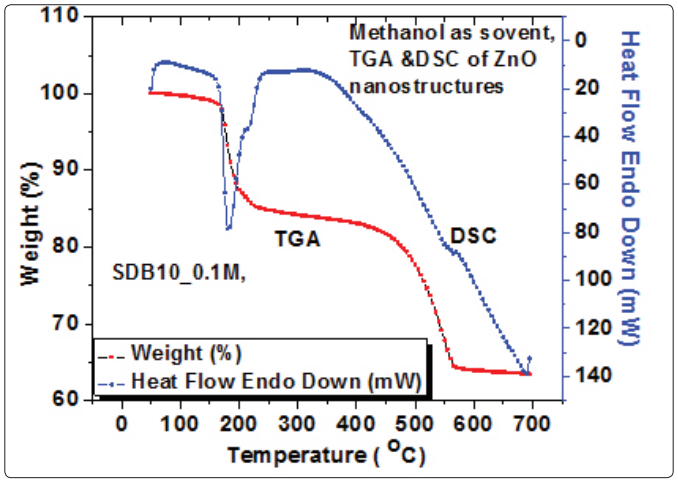

Figure 4(d): TGA & DSC curves of SDB10

TGA and DSC analyses of ZnO nanostructures were carried out using Simultaneous Thermal Analyzer: STA 6000, Perkin Elmer U.S.A. Approximately 30 mg of the sample was placed in a platinum crucible on the pan of the microbalance and heated from 50 °C to 700°C using Al_2O_3 as inert material. Analysis was performed under nitrogen flow (flow 20ml/min) at heating rate of 20°C/min.

Figure 4(a) shows TGA and DSC curves of SDB5 sample ($ZnCl_2$ 0.25M and NaOH 2.5M). Very small weight loss of 3.5% was observed. Weight loss may be due to evaporation of adsorbed water vapours on ZnO powder particles. There is no endothermic peak on DSC curve, which indicates the formation of stable ZnO phase.

Figure 4(b) shows TGA and DSC curves of SDB8 sample ($ZnCl_2$ 0.25M and NaOH 0.5M). There was a weight loss of 4.2%. There is no endothermic peak on DSC curve. It may also be due to stable and homogeneous ZnO phase. Weight loss may be due to evaporation of adsorbed water vapours on ZnO.

Figure 4(c) shows TGA and DSC curves of SDB11 sample ($ZnCl_2$ 0.25M and NaOH 0.25M). There is the weight loss of 32% and DSC curve shows one major endothermic peak from 160 °C to 230 °C. The loss of weight and endothermic peak may be due to dissociation of intermediate species, such as, $Zn(OH)_2$ and evaporation of water vapours with byproducts.

TGA curve and DSC curves of SDB10 sample are shown in figure 4(d). There is the weight loss of 36.5 % and DSC curves shows one large endothermic peak from 170 °C to 215 °C. The loss of weight and endothermic peak may be due to dissociation of $Zn(OH)_2$ and evaporation of water vapours with byproducts.

It is clear from TGA and DSC curves in figures 4(a) and 4(b) that the stable and homogeneous ZnO nanostructures (nanoparticles or nanorods) can be synthesized when the molarity of NaOH was above 0.5M ($ZnCl_2$/NaOH should be smaller than 0.5).

Optical properties of ZnO Nanoparticles

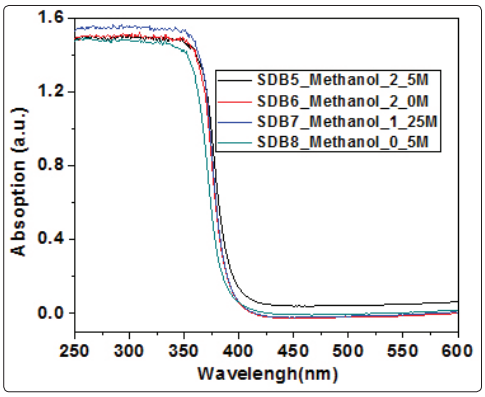

Figure 5(a): UV-Vis absorption spectra of ZnO nanoparticles

Figure 5(a) shows UV-Vis absorption spectra of ZnO nanostructured samples. Band gap energy of SDB5, SDB6, SDB7 and SDB8 was observed to be 3.44, 3.47, 3.49 and 3.51eV respectively. The observed band gap energies were larger than reported band gap energy (3.37eV).

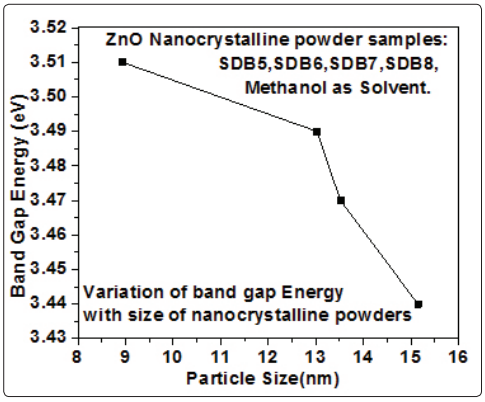

Figure 5(b): Variation of band gap energy with size of ZnO nanoparticles

The band edges of SDB5, SDB6, SDB7 and SDB8 were shifted towards lower wavelength side. There was blue shift in edge wavelength for each sample. This indicates the nanocrystalline nature of as prepared ZnO samples. Band gap energy is increasing with decrease of grain size as shown in Figure 5(b).

Photoluminescence characteristics of ZnO Nanoparticles

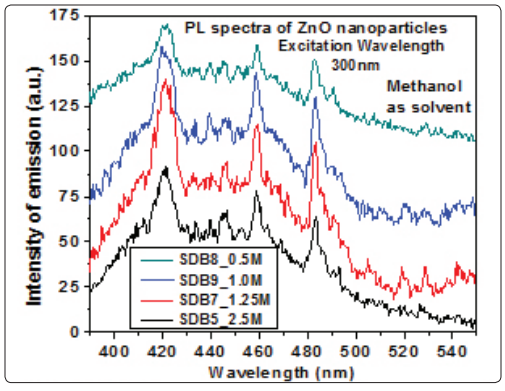

Figure 6(a): PL spectra of ZnO nanoparticles

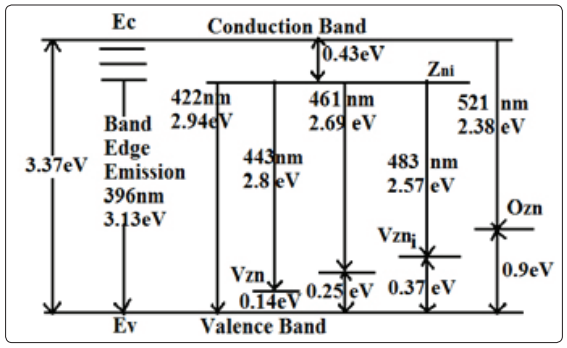

Figure 6(b): Schematic representation of PL

Figure 6(a) illustrates the room temperature photoluminescence spectra of ZnO nanostructures at excitation wavelength of 300 nm. The schematic representation of the emission peaks at: ~396nm, ~422 nm, ~ 443nm, ~ 461nm ~ 483nm and ~ 521 nm in ZnO nanostructures is shown in Figure 6(b). It is commonly considered that band edge emission at ~396 nm may be due to the recombination of excitons [23]. Defect related major emission bands were observed as: violet emission at 422 nm (~2.94 eV), indigo emission at 443nm (~2.8 eV), blue emission at 461 nm (~2.69 eV), blue–green emission at 483 nm (~2.57 eV) and green emission at 521 nm (~2.38 eV). Visible emissions in ZnO may be due to different intrinsic defects such as oxygen vacancies Vo, zinc vacancies VZn, oxygen interstitials Oi, zinc interstitials Zni and oxygen antisites OZn. The origin of violet emission (422 nm (~2.94 eV) may be ascribed to an electron transition from a shallow donor level of neutral Zni to the top level of the valence band [24]. Therefore, the shallow donor level of the Zni is suggested to locate at ~0.43 eV below conduction band. A indigo (violet-blue) emission centered at 443 nm (~2.8 eV) may be due to a radiative transition of an electron from the shallow donor level of Zni to an acceptor level of neutral VZn [25]. The acceptor level of VZn may locate at ~0.14 eV above the valence band. The blue emission at around 2.69 eV (461 nm) may be related to surface defects of ZnO nanostructure located at ~0.25 eV above the valence band. Blue–green emission at 483 nm (~2.57 eV) may be due to intrinsic VZni [26]. The possible reason for observed green emission in ZnO nanostructures may be due to radiative transition from conduction band to the edge of the acceptor levels of Ozn caused by oxygen antisites OZn [27, 28]. As the peak position of the green emission is at ~2.38 eV (521 nm), the acceptor level of the oxygen antisites OZn may be located at ~0.9 eV above the valence band.

Discussion

The solvent in the chemical route technique must have a relatively high dielectric constant so that it can dissolve the inorganic salts like zinc chloride [29-31]. Most alcohols are dipolar and amphiprotic with a dielectric constant that depends on the chain length [32]. Alcohols with low carbon number, up to 4, are mostly used as solvents such as methanol, ethanol, 1-propanol, 2-propanol, 1-butanol and 2-methoxyethanol. Methanol was used as solvent in present investigation. Zinc chloride was more soluble in methanol than in ethanol or 2- methoxyethanol according to dielectric constants of these alcohols.

The formation of ZnO colloidal particles in an alcoholic solvent consists of two stages [33-35]: (i) Ostwald ripening- large particles grow at the expense of smaller particles (smaller particles have

a higher solubility) and, (ii) an aggregation. During the early stage of phase transformation, small oligomers (smallest stable molecular clusters) are continuously formed. At advanced stages, the aggregation of the oligomers leads to crystalline wurtzite -the primary colloidal particles. The primary particles then aggregate and form the secondary colloidal particles. It has been reported that at least four different 'primary particles or clusters', serving as initiators of the ZnO colloid growth, could be identified [36]. The nature of these 'primary particles or clusters' depends strongly on the synthesis conditions chosen viz. initial salt concentration, the temperature, time of the thermal treatment, the nature of alcohol solvent and humidity. The kinetics of nucleation and growth are expected to be strongly dependent on the properties of the solvent. For the shorter chain length, alcohols (ethanol and 1-propanol) nucleation and growth are retarded as compared to longer chain length alcohols (from 1- butanol to 1-hexanol) where nucleation and growth are fast. The particles size increases with increasing temperature for all solvents and increases with alcohols chain length. In fact, during the growth of colloidal ZnO nanoparticles, the alcohols not only provide the medium for the reactions, but also act as ligands to help control the morphology and particle size of ZnO.

Various researchers suggested that NaOH concentration plays a vital role in determining the morphology, size and optical band gap of obtained nanostructures [37-39]. The survey of many significant reports reveals that the size of the nanostructures is directly proportional to NaOH concentration where the particle size increases accordingly [40-42]. It is clear from SEM images that the particle size is larger when NaOH concentration is higher (Figure 3(a) to (d)). This phenomenon is explained in terms of Ostwald ripening [43, 44]. According to this, under synthesis conditions, tiny crystallites nucleate first and then they agglomerate into larger crystallites due to the energy difference between large and smaller particles of higher solubility based on Gibbs-Thomson law [45]. It can be seen from the SEM images in figure 3 that NaOH concentration had a great influence on the morphology of the ZnO nanorods. It is known that Zn2+ ions react with the OH− ions by following mechanisms:

(a) Formation of ZnO nuclei

$$ZnCl_2 + 2H_2O \rightarrow Zn^{2+} + 2OH^- + 2HCl \quad (1)$$

$$NaOH + 2H_2O \rightarrow Na^+ + 3OH^- + 2H^+ \quad (2)$$

$$Zn^{2+} + 2OH^- \rightarrow ZnO\ (Nuclei) + H_2O \quad (3)$$

(b) Growth-Dissolution Recrystallization:
Subsequently, ZnO nanostructures undergo a reversible dissolution and recrystallization process via formation of $Zn(OH)_2$, leading to formation of one dimensional (1D) ZnO microrods.

$$ZnCl_2 + 2NaOH \rightarrow Zn(OH)_2 + 2NaCl + 2H_2O \quad (4)$$

$$Zn(OH)_2 + 2H_2O = Zn^{2+} + 2OH^- + 2H_2O \rightarrow Zn(OH)_4^{2-} \quad (5)$$

$$Or,\ Zn(OH)_2 + 2OH^- \rightarrow Zn(OH)_4^{-2} \quad (6)$$

$$Zn(OH)_4^{2-} \leftrightarrow ZnO_2^{-2} + 2H_2O \quad (7)$$

$$ZnO_2^{-2} + 2H_2O \leftrightarrow ZnO + 2OH^- \quad (8)$$

When concentration of Zn^{2+} and OH^- reaches to super saturation, ZnO nuclei would form. The zinc chloride would convert into $Zn(OH)_2$ colloids first in alkali solution. During the process, part of $Zn(OH)_2$ colloids would dissociate into Zn^{2+} and OH^-. The $Zn(OH)_2$ clusters dissolve in Zn^{2+} and OH^- ions which form the $Zn(OH)_4^{2-}$ complexes. When the concentration of these growth units ($Zn(OH)_4^{2-}$ complexes) exceeds the critical super saturation level, the growth units become ZnO nuclei spontaneously in the solution.

The pH values of mixture solutions while preparing SDB5, SDB6, SDB7, SDB9 and SDB8 were measured to be 10.8, 10.5, 9.9, 9.5 and 9.3 respectively. The average grain size of ZnO nanostructures is observed to be decreasing with decreasing pH as indicated in Table 2 and also from SEM images. When solution pH is larger, the solution would be thicker, mobility of growth unit would be smaller and the rate of growth would be slower. This could be one of reasons of growth of nanorods or elongated nanoparticles when ratio of $ZnCl_2$/NaOH is 0.1, 0.2 and 0.25.

When the nucleation rate is faster, the resulting particle size is smaller. When ratio of $ZnCl_2$/NaOH is 0.5 in case of SDB8 sample, the concentration of OH^- ions would be relatively smaller as compared to the mixture solutions corresponding to SDB5, SDB7 and SDB9 samples. Hence, ZnO nucleation centres would be larger. The growth units ($Zn(OH)_4^{2-}$ would be distributed on these ZnO nucleation centres and ZnO nanoparticles of almost uniform size (monodisperse) were possible as shown figure 3(d) [46].

Conclusions

- Morphology and size of ZnO nanostructures were controlled by controlling NaOH concentration.
- Aspect ratio of nanorods was observed to be 3.76 when molarity of NaOH was 2.5M and was 4.63 when molarity was 1.25M.
- When molarity of NaOH was decreased to 1.0M, the rods like particles were changed to elongated shape.
- The length and diameter of elongated particles were decreased and the aspect ratio was 1.68.
- With further decrease of molarity of NaOH to 0.5M, the growth along c axis ceased and spherical particles of average size of 8.9nm (as determined from Debye Scherrer formula) and was 13nm (as determined from SEM image in figure 3(d)) were obtained. In synthesis process of ZnO nanoparticles, atomized $ZnCl_2$ solution (methanol as solvent) was used to mix in NaOH solution (methanol as solvent) to avoid dendritic growth (flower like structures) of ZnO nanostructures.
- Repeatability in synthesizing monodisperse ZnO nanoparticles was observed when molarity of NaOH was 0.5M (and above) and molarity of $ZnCl_2$ solution was 0.25M.
- When molarity of NaOH was decreased to 0.25M (keeping molarity of $ZnCl_2$ solution same (0.25M)), it was not possible to obtain the homogeneous phase of ZnO.
- Ultrasonically atomized precursor assisted simple chemical route was cost effective technique having potential to synthesize monodisperse ZnO nanoparticles on large scale.

Acknowledgements

The authors are grateful to the Principal, Pratap College Amalner for providing laboratory facilities and thankful to the Head, P. G. Department of Physics and the Principal, Pratap College Amalner for their support for pursuing the research. One of us (Miss D. G. Patil) is grateful to Department of Science and Technology, Govt.

of India, for providing INSPIRE Fellowship.

References

1. Dabrowski B, Zaleska A, Janczarek M, Hupka J, Miller JD (2002) Photo-oxidation of dissolved cyanide using TiO_2 catalyst. J Photochem Photobiol A Chem 8: 201-205.
2. Kobayashi H, Liu YL, Yamashita Y, Ivanco J, Imai S, et al. (2006) Methods of observation and elimination of semiconductor defect states. Sol Energy 8: 645-652.
3. Rao AN, Sivasankar B, Sadasivam V (2009) Kinetic study on the photocatalytic degradation of salicylic acid using ZnO catalyst. J Haz Mat 8: 1357-1361.
4. Liu J, Zhao Y, Jiang YJ, Lee CM, Liu YL, et al. (2010) Identification of zinc and oxygen vacancy states in nonpolar ZnO single crystal using polarized photoluminescence. Appl Phys Lett 8: 231907-231909.
5. Zhao L, Lu PF, Yu ZY, Guo XT, Shen Y, et al. (2010) The electronic and magnetic properties of (Mn, N)-codoped ZnO from first principles. J Appl Phys 8: 113924-113930.
6. Chou MMC, Hang DR, Chen C, Wang SC, Lee CY (2011) Nonpolar a-plane ZnO growth and nucleation mechanism on (100) (La, Sr)(Al, Ta)O_3 substrate. Mater Chem Phys 8: 791-795.
7. Xu SJ, Liu W, Li MFL (2002) Direct determination of free exciton binding energy from phonon-assisted luminescence spectra in GaN epilayers. Appl Phys Lett 8: 16-18.
8. Byeong Woo Lee, Jin Heui Koo, Tae Suk Lee, Yun Hae Kim, Jae Suk Hwang (2013) Synthesis of ZnO Nanoparticles via Simple Wet-Chemical Routes. Advanced Materials Research 699: 133-137.
9. Zhu BL, Zhao XZ, Suc FH, Li GH, Wu XG, et al. (2010) Low temperature annealing effects on the structure and optical properties of ZnO films grown by pulsed laser deposition. Vacuum 8: 1280-1286.
10. Yang Z, Lim JH, Chu S, Zuo Z, Liu JL (2008) Study of the effect of plasma power on ZnO thin films growth using electron cyclotron resonance plasma-assisted molecular-beam epitaxy. Appl Surf Sci 8: 3375-3380.
11. Sohal S, Alivov Y, Fan Z, Holtz M (2010) Role of phonons in the optical properties of magnetron sputtered ZnO studied by resonance Raman and photoluminescence. J Appl Phys 8: 053507-053511.
12. Wu C, Shen L, Huang Q, Zhang YC (2011) Synthesis of Na-doped ZnO nanowires and their antibacterial properties. Powder Technol 8: 137-142.
13. Chang SS, Park CH, Park SW (2003) Improved photoluminescence properties of oxidized anodically etched porous Zn. Mater Chem Phys 8: 9-14.
14. Hussein AK (2015) Applications of nanotechnology in renewable energies-A comprehensive overview and understanding. Renewable and Sustainable Energy Reviews 42: 460-476.
15. Hussein AK, Walunj A, Kolsi L (2016) Applications of nanotechnology to enhance the performance of the direct absorption solar collectors, Journal of Thermal Engineering 2: 529-540.
16. Li D, Li Z, Zheng Y, Liu C, Hussein AK, et al. (2016) Thermal performance of a PCM-filled double-glazing unit with different thermophysical parameters of PCM. Solar Energy 133: 207-220.
17. Hussein AK (2016) Applications of nanotechnology to improve the performance of solar collectors – Recent advances and overview, Renewable and Sustainable Energy Reviews 62: 767-792.
18. Hussein AK, Li D, Kolsi L, Kata S, Sahoo B (2017) A review of nano fluid role to improve the performance of the heat pipe solar collectors. Energy Procedia 109: 417- 424.
19. Chand R, Rana G, Hussein AK (2015) on the onset of thermal instability in a low Prandtl number nanofluid layer in a porous medium. Journal of Applied Fluid Mechanics 8: 265-272.
20. Chand R, Rana G, Hussein AK (2015) Effect of suspended particles on the onset of thermal convection in a nanofluid layer for more realistic boundary conditions. International Journal of Fluid Mechanics Research 42: 375-390.
21. Hussein AK, Mustafa A (2018) Natural convection in a parabolic enclosure with an internal vertical heat source filled with Cu–water nanofluid. Heat Transfer-Asian Research 47: 320-336.
22. Al-Rashed A, Kalidasan K, Kolsi L, Aydi A, Malekshah E, et al. (2018) Three-dimensional investigation of the effects of external magnetic field inclination on laminar natural convection heat transfer in CNT-water nanofluid filled cavity. Journal of Molecular Liquids 252: 454-468.
23. Vanheusden K, Warren WL, Seager CH, Tallant DR, Voigt JA, et al. (1996) Mechanisms behind green photoluminescence in ZnO phosphor powders. J Appl Phys 79: 7983-7990.
24. Fan XM, Lian JS, Zhao L, Liu Y (2005) Single violet luminescence emitted from ZnO films obtained by oxidation of Zn film on quartz glass. Appl Surf Sci 252: 420-424.
25. Tatsumi T, Fujita M, Kawamoto N, Sasajima M, Horikoshi Y (2004) Intrinsic defects in ZnO films grown by molecular beam epitaxy. Jpn J Appl Phys 43: 2602-2606.
26. Ding Xi, Yanjun Fang, Haolei Qian, Ming Zhao, Wei Wang, et al. (2016) Influence of the precursor anion on the photoluminescence properties of ZnO. Optic Express 24: 25876-25884.
27. Lin B, Fu Z, Jia Y (2001) Green luminescent center in undoped zinc oxide films deposited on silicon substrates. Appl Phys Lett 79: 943-945.
28. Murphy TE, Moazzami K, Phillips JD (2006) Trap−related photoconductivity in ZnO epilayers. J Electron Mater 35: 543-549.
29. MZ Hu, EA Payzant, CH Byers (2000) Sol-Gel and Ultrafine Particle Formation via Dielectric Tuning of Inorganic Salt-Alcohol-Water Solutions. J Colloid Interface Sci 222: 20-36.
30. Hosono E, Fujihara S, Kimura T, Imai H (2004) Non-Basic Solution Routes to Prepare ZnO Nanoparticles. Journal of Sol-Gel Science and Technology 29: 71-79.
31. D Sun, M Wong, L Sun, Y Li, N Miyatake, et al. (2007) Purification and stabilization of colloidal ZnO nanoparticles in methanol. J Sol Gel Sci Technol 43: 237-243.
32. Z Hu, G Oskam, PC Searson (2003) Influence of solvent on the growth of ZnO nanoparticles. J Colloid Interface Sci 263: 454-460.
33. L Spanhel, MA Anderson (1991) Semiconductor clusters in the sol-gel process: quantized aggregation, gelation, and crystal growth in concentrated zinc oxide colloids. J Am Chem Soc 113: 2826-2833.
34. EA Meulenkamp (1998) Synthesis and Growth of ZnO Nanoparticles. J Phys Chem B 102: 5566-5572.
35. MS Tokumoto, SH Pulcinelli, CV Santilli, AF Craievich (1999) SAXS study of the kinetics of formation of ZnO colloidal suspensions. J Non-Cryst Solids 247: 176-182.
36. L Spanhel (2006) Colloidal ZnO nanostructures and functional coatings: A survey. J Sol Gel Sci Technol 39: 7-24.

37. Sonia S, Jayram ND, Suresh Kumar P, Mangalaraj D, Ponpandian N, et al. (2014) Effect of NaOH concentration on structural, surface and antibacterial activity of CuO nanorods synthesized by direct sonochemical method. Superlattice Microst 66: 1-9.
38. Moazzen MAM, Seyed MB, Forshaw T (2013) Change in the morphology of ZnO nanoparticles upon changing the reactant concentration. Appl Nanosci 3: 295-302.
39. Anandhavelu S, Thambidurai S (2011) Effect of zinc chloride and sodium hydroxide concentration on the optical property of chitosan–ZnO nanostructure prepared in chitin deacetylation. Mater Chem Phys 131: 449- 454.
40. Chand P, Gaur A, Kumar A, Gaur UK (2015) Effect of NaOH molar concentration on optical and ferroelectric properties of ZnO nanostructures. Appl Surf Sci 356: 438-446.
41. Xu S, Wang ZL (2011) One-dimensional ZnO nanostructures: Solution growth and functional properties. Nano Res 4: 1013-1098.
42. Umar A, Hahn YB (2010) ZnO Nanoparticles: Growth, Properties and Applications in, Umar A., Hahn Y.B. (Eds.), Metal Oxide Nanostructures and Their Applications, American Scientific Publishers, California 4: 1-34.
43. Polsongkram D, Chamninok P, Pukird S, Chow L, Lupan O, et al. (2008) Effect of synthesis conditions on the growth of ZnO nanorods via hydrothermal method. Physics B 403: 3713-3717.
44. Li WJ, Shi EW, Zheng YQ, Yin ZW (2001) Hydrothermal preparation of nanometer ZnO powders. J Mater Sci Lett 20: 1381-1383.
45. Wang L, Muhammed M (1999) Synthesis of zinc oxide nanoparticles with controlled morphology. J Mater Chem 9: 2871-2878.
46. Sepulveda-Guzman S, Reeja-Jayan B, Rosa E, Torres-Castro A, Gonzalez-Gonzalez V, et al. (2009) Synthesis of assembled ZnO structures by precipitation method in aqueous media. Mater Chem Phys 115: 172-178.